IIR Filter Models of Haptic Vibration Textures

Vijaya Lakshmi Guruswamy, Jochen Lang, *Member, IEEE,* and Won-Sook Lee, *Member, IEEE*

***Abstract*—Haptic tactile feedback is a widely used and effective technique in virtual reality applications. When an object's surface is explored by stroking it using fingers, finger nails or a tool, a vibration response is sensed. The vibrations convey information about the surface finish and patterns in the surface structure, and they may help to identify the surface. We study characteristics of real-world, physical objects based on actual measurements. We propose novel techniques for modeling haptic vibration textures using digital filters which can simulate both stochastic and patterned textures of objects. The modeling is based on a spatial distribution of infinite-impulse-response filters which operate in the time domain. We match the impulse response of the filters to acceleration profiles obtained from scanning of real-world objects. The results show our modeling is efficient in representing varying roughness characteristics of both regular-patterned surfaces and stochastic surfaces unlike prior methods based on a parametric decaying sinusoid model. Our experiments employ an existing hand-held mobile scanning set-up with a visually-tracked probe, which provides acceleration and force profiles. Our simple capturing devices also remove any need for a robotic manipulator.**

***Index Terms*—Virtual reality, user interfaces, vibrations, IIR digital filters, haptics, texture modeling.**

I. Introduction

Haptic perception is one way for humans to become aware of their physical surroundings. Our research interest lies in assisting haptic perception in virtual environments when a user touches a virtual object. In this paper, we discuss parameterization of vibrotactile feedback in haptic rendering of texture scans. Vibrotactile feedback in reality-based virtual environments increases realism [1]. Reality-based models are created using data acquired from real environments by employing various sensors [2]. We focus on modeling of vibrotactile signals based on measurements, and in particular, a modeling method which is applicable to an extended range of object categories. The goals of modeling are to extract texture characteristics of an object which distinguish it from other objects and to have flexibility in rendering. Our models can render different paths, with various traversal speeds and user forces and in combination with modified or enhanced haptic object characteristics, e.g., object deformations or friction.

The authores are with the School of Information Technology and Engineering, University of Ottawa, Ottawa, Canada ON K1N 6N5. e-mail: jlang@site.uottawa.ca, wslee@site.uottawa.ca

Manuscript received Decemeber 15, 2009, revised June 10, 2010, accepted July 15, 2010. This work was supported by the Natural Sciences and Engineering Research Council of Canada. The Associate Editor coordinating the review process for this paper was Dr. A. Sarti.

Digital Object Identier 10.1109/TIM.2010.2065751

Vibration signals contribute significantly to tactile perception when we have physical contact to our environment through a tool as shown by Klatzky and Lederman [3]. Vibrations are generated, e.g., as we scan across a surface which activates somatosensory receptors in the skin, e.g., the Pacinian corpuscle with a peak sensitivity of 250 Hz. Vibration feedback can also be generated with very simple means and it is used in game controllers, cellphones and mobile devices because of its efficacy [4]. In early work, Wellman and Howe [5] recorded vibration waveforms during tapping on surfaces and played the waveforms back through a haptic interface. The pervasiveness of vibrations has motivated Okamura et al. [6] to extend the above vibrotactile model to a wider array of material interactions from tapping to membrane puncture in medical training applications and to stroking textures with a stylus. They showed that the vibration feedback model alone enhanced the realism of haptic textures. Since then tapping, e.g., Kuchenbecker et al. [7] and needle insertion [8] have received a great amount of attention. However, despite the fact that Okamura et al. had reported that their subjects perceived vibration-based textures as most realistic, vibrotactile textures have only been further investigated in our work [9] and in the parallel work of the research group of Kuchenbecker et al. [10], [11].

Okamura et al. [6] classify haptic textures as either general or patterned. General textures are stochastic without any discernible features, e.g., sandpaper, while patterned textures have regular distinguishable features, e.g., grooves. Okamura et al. fit a decaying sinusoid to the acceleration profile in the time domain generated by stroking over a surface groove. They also identify the major frequency in the acceleration profile for general textures. Our experiments confirm their observation that features cause a decaying impulse-response when stroking a surface. However, we develop a novel unified filtering method for both kinds of surfaces, general and patterned. Instead of a decaying sinusoid to model the accelerations, we use an infinite-impulse filter (IIR). This allows the use of a higher order filter to capture more than just the major frequency of the response, as well as to extend the haptic texture model to arbitrary surfaces including stochastic textures. Our unified model works for any surface and is simple to render with low latency because of the computational simplicity of IIR filters.

We estimate our IIR model parameters from profiles of force and acceleration collected by stroking real-world surfaces with a wireless haptic texture sensor, the WHaT [12] with integrated visual tracking [13]. We utilize a scanning approach

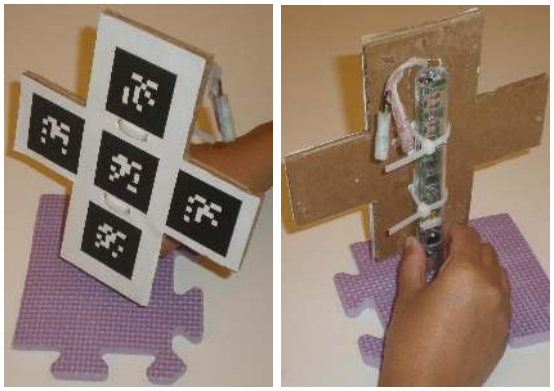

Fig. 1. Scanning with the WHaT.

developed by Lang and Andrews [14] for our novel vibrotactile measurements and modeling, which is not the subject of this paper. Most importantly, our scanning set-up has the ability to collect force and acceleration profiles from free-form surfaces and our models can be estimated from surfaces measured on-site (see Figure 1).

This paper is a greatly extended version of our preliminary workshop paper [9] and our main contributions and improvements are: (i) We present a new segmentation method of the scanned acceleration signal where most segments correspond to an intuitive part of a texture scan without over- or under-segmentation. This results in many fewer IIR filters needed to model the same section of the surface compared to the previous method presented in the workshop. (ii) We have conducted many more experiments where we scanned different objects with different tangential velocities and modeled the velocity dependency of the acceleration response.

The remainder of this paper is organized as follows: Section II provides a discussion of haptic textures. We present in Section III our IIR-lter-based haptic texture model along with a discussion of rendering approaches. Section IV details the estimation of IIR-filter parameters from our measurements, both, for a single feature of a texture and for a complete profile. Section V presents estimated profiles for different types of surfaces. We conclude our paper in Section VI with some future directions.

II. Background and Related Work

Haptic textures are a common part of virtual environments and many different modelling and rendering approaches exist. Tactile sensing may also be used for other tasks, e.g., recognition [15] and geometric profiling [16]. In their sandpaper system, Minsky et al. [17] render forces based on the gradient of the local surface. The surface texture is either represented procedurally or by an image. Since then, many different approaches have been suggested. Siira and Pai [18] use normal variations derived from surface roughness parameters for their stochastic textures. Basdogan et al. [19] model textures as bump maps which are either derived procedurally or from images similar to computer graphics. Wall and Harwin [20] employ Fourier series to represent a spatial frequency response measured during surface profiling while Costa and Cutkosky [21] simulate surface height profiles with fractals. We are motivated to explore vibrotractile textures by Klatzky and Lederman [3] who state that their "findings support the use of vibrotactile cues to roughness in environments in which direct skin contact is precluded". Commercial pen-like haptic devices do not simulate skin contact and hence our pursuit of vibrotactile textures.

Wellman and Howe [5] studied ways to convey the stiffness of virtual objects based on measured vibration waveforms during a tapping experiment. Their work demonstrated that high frequency vibrotactile feedback can effectively alter the way objects are perceived in a virtual environment. Okamura et al. [6] extended the vibrotactile model to acceleration profiles sensed during stroking of a surface. Their model is a decaying sinusoid which is fit in the time-domain to an acceleration profile acquired when passing a groove in the surface. We extend in our work the vibration feedback model to arbitrary surfaces using a more general decaying impulse response represented by an IIR filter. McMahan et al. [22] have very recently shown that acceleration feedback enhances realism when remotely probing textures as long as some stiffness is rendered as well. In their study users rated vibration-augmented rendering of samples as more realistic than position controlled interactions. The most closely related work to ours is the simultaneous work by Kuchenbecker et al. [10] who also fit the coefficients of digital filters to acceleration waveforms. In their work, they adapt an approach from audio processing where the output of a linear predictor in response to a white noise input is matched to a measured signal. Although the work reported in [10] does not contain a segmentation method of the acceleration waveforms, the same research group has been working on a more general texture modeling technique simultaneously to us [11].

Our model is also closely related to the earlier event-based haptics approach by Kuchenbecker et al. [7] who model the vibrations during tapping by acceleration matching based on measurements. In acceleration matching the transfer function between force and accelerations is estimated from tapping on samples with the stylus of an instrumented haptic device. During rendering with the same stylus-based device the transfer function is used to generate open-loop vibration transients.

We render our vibration textures also with standard stylus-based haptic devices, but simpler devices based on a tractor or inertial motor may be effective as well. According to Hayward and MacLean [4] these types of vibrotactile devices are the most common way to render vibrotactile feedback today and can be found in pagers, cellphones and game controllers. McMahan et al. [1] augment a consumer haptic device, a Phantom Omni®, with a linear actuator enabling the rendering of vibration waveforms in addition to haptic rendering of tool contact.

III. IIR Filter Model

We designed our haptic texture model based on the force and acceleration profiles which we have observed in scanning surfaces with the WHaT [18]. The WHaT is a stylus-like instrument which records three-dimensional accelerations and

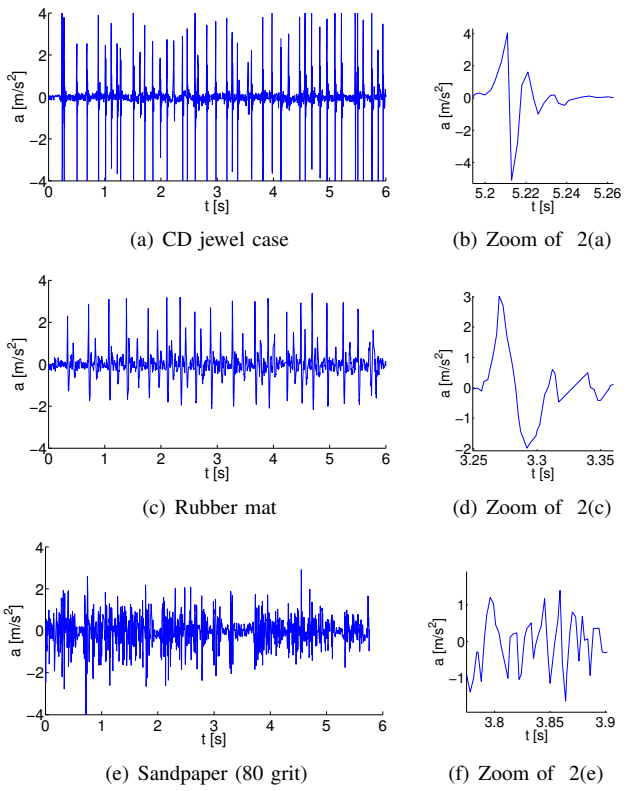

(a) CD jewel case (b) Zoom of 2(a)

(c) Rubber mat (d) Zoom of 2(c)

(e) Sandpaper (80 grit) (f) Zoom of 2(e)

Fig. 2. Measured Acceleration Profiles. (Time scale is variable.)

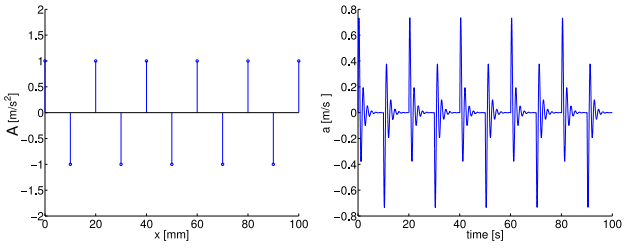

(a) Filter locations and amplitude (b) Constant velocity response

Fig. 3. Haptic texture model with filters due to surface features located in space and damping over time (tutorial figure showing damped sinusoids with amplitudes $A = \pm 1\mathrm{m/s}^2$).

the force along its major axis. The values are transmitted via a wireless link to a host PC at about 500 Hz. Simultaneously, we visually track fiducial markers on the pen (see Figure 1) with a stationary camera at about 100 Hz. The system is described in detail in [13], [14] and has several advantages over commercial profilers and vibration testers. Mobile profilers measure surface height variations for roughness determination but typically do not record accelerations while mobile vibration testers are meant to be kept stationary and both types of instruments do not record forces.

Figure 2 shows three different acceleration profiles normal to the surface that resulted from scanning a rubber mat, a CD jewel case, and sandpaper (80 grit). We selected these objects because they are representative of different types of surfaces. A CD jewel case contains regular ridges and grooves on the scanned thin side and these are recognizable in the acceleration profile in Figure 2(a). The rubber mat consists of a pattern of repeating shapes which are discernible in the acceleration profile in Figure 2(c) but mixed with a more stochastic pattern. The accelerations when scanning sandpaper in Figure 2(e) are stochastic without any repeatable pattern. The measured profiles have already been processed, i.e., the x, y and z accelerometer readings combined with the measured orientation of the WHaT have been used to estimate the acceleration normal to the scanned surface (see [13] for a system description). The profiles have also been normalized for variations in applied force. We use the linear coefficients k_c of Lang and Andrews [14] which relate the root-mean-squared accelerations a_{RMS} to the lowpass-filtered measured force $f_{lowpass}$ by

$$a_{RMS} = k_c * f_{lowpass} + a_0. \tag{1}$$

Lang and Andrews [14] have shown that the proportionality constant k_c is related to the reduced Young's modulus of compliant material measured during compression. They report $k_c = 0.117$ for the rubber mat and $k_c = 0.526$ for the tire tread. We use $k_c = 1.0$ for rigid surfaces, i.e., the jewel-case as well as for the different sandpapers. The mean forces in the scans shown in Figure 2 are $\bar{f} = 0.443$ N, $\bar{f} = 0.874$ N and $\bar{f} = 0.353$ N for the rubber mat, CD jewel-case and the sandpaper, respectively.

Okamura et al. [6] have shown that the amplitude of the transient accelerations observed during tapping is linearly related to the "attack velocity". We experimentally observe similar behavior for the relationship between the RMS acceleration and the tangential velocity during surface stroking. We extend Equation 1 to include this relationship and hence

$$\tilde{a}_{RMS} = k_v * v_t + k_c * f_{lowpass} + \tilde{a}_0. \tag{2}$$

We find values for $\tilde{a}_0$ and k_v by linear regression based on multiple scans of the same surface with different velocity. We use the same proportionality constant k_c as Andrews and Lang [14]. Our results are detailed in Section V.

When a surface is scanned with the probe, an acceleration pulse occurs at locations of texture features on the surface. Inspired by Okamura et al. [6], we model such a pulse as the initial peak of a decaying vibration wave, i.e., the feature triggers a vibration at a certain location on the surface which then diminishes over time. Okamura et al. used a decaying sinusoid to represent this relation in the time domain as

$$a(t) = Ae^{-\beta t} \sin \omega t \tag{3}$$

where A, β and $\omega = 2\pi f$ represent the amplitude, the decay rate and the angular frequency of the waveform, respectively. They applied their model only to surfaces with features (grooves). Decaying impulse responses over time are located at feature locations in space. Figure 3 shows a synthetic example of our interpretation of such a haptic texture model. The model consists of ten filters, each with a response according to Equation 3. Figure 3(a) depicts the distribution of the filters over the surface. Figure 3(b) shows the corresponding acceleration profile if the surface is traversed with constant speed.

Instead of using the continuous relationship of Equation 3, we use the impulse response of a discrete filter to represent the acceleration signal because when rendering haptic textures, the impulse response will be created in software. We model the system with a discrete IIR filter with a sampling period T. Assuming that the vibrations can be described by a decaying sinusoid, then the Z-transform of the IIR filter is given by

$$H(z) = A\frac{ze^{-\beta T}\sin(\omega T)}{z^2 - 2ze^{-\beta T}\cos(\omega T) + e^{-2\beta T}} \tag{4}$$

The filter generates the desired vibration pattern at each feature location by simply putting an impulse into the filter. The coefficients of the IIR filter model can be chosen differently from Equation 4. We design the IIR filter such that its impulse response matches the acceleration profile which we have measured stroking the surface with the WHaT. We discuss how to find the filter coefficients in Section IV.

A. Haptic Texture Rendering

For haptic rendering of our texture, we adapt the model of Andrews and Lang [23] in which a scanning profile is registered with a triangular surface mesh. A point on the surface is parametrized as a position along the 1D scanning profile and a distance normal to the profile. Haptic rendering employs a penalty-based approach where the penalty force is composed of a rigid body constraint force plus a texture force normal to the surface plus a tangential frictional force. We use the same force terms as Andrews and Lang [23] but instead of a texture force based on rendering a height profile, we directly use the scaled acceleration profile generated by the IIR filter as texture force. Our texture force is the sum of K currently active filters scaled by A_k. A filter becomes active once the haptic interaction point has traversed the filter location x_k on the profile at a discrete time prior to the current sampling time. The k^{th} filter response must therefore be shifted by $-t_k = -cT$ and the overall normal texture force is then given by

$$F_t(z) = \sum_{k=0}^{K} A_k z^{-t_k/T} H_k(z) \tag{5}$$

where

$$H_k(z) = \frac{\sum_{i=0}^{M_k} b_{ik} z^{-i}}{\sum_{i=0}^{N_k} a_{ik} z^{-i}}$$

with $M_k \leq N_k$ and $a_{0k} = 1$ for all filters.

We attempted to render our texture with a stylus-based haptic device with a haptic update rate close to 1 kHz. However, the actual upper frequency which can be felt by the user is much lower due to the limited bandwidth of the device. We believe that the use of a separate voice-coil vibrator as proposed by McMahan and Kuchenbecker [10] is a superior approach. The open-loop rendering method by Kuchenbecker et al. [7] could also be adapted to render the accelerations without augmenting the handle of the haptic device.

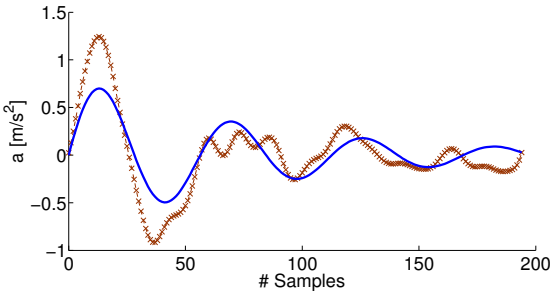

(a) Decaying Sinusoid Model

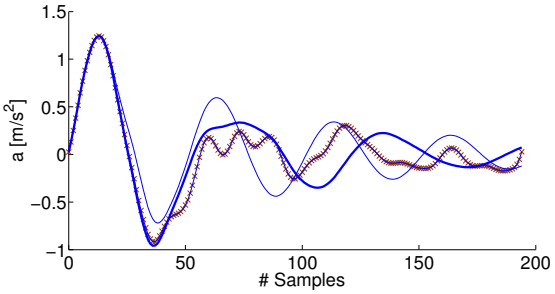

(b) Prony's Method

Fig. 4. Estimation of IIR filter model. Bandpass filtered measurements are marked with a cross, the solid lines are filter responses. The result of a time domain estimation for a decaying sinusoid is shown in 4(a), the result of Prony's method with $N = M = 11$, $N = M = 16$ (bold), and $N = M = 106$, respectively are shown in 4(b). The IIR filter with $N = M = 16$ is the one used in our approach since it is the filter with the smallest number of coefficients for an average absolute sum of acceleration error of less than $0.153\,\mathrm{m/s^2}$ and $N = M$.

IV. Model Estimation

In this section, we discuss the procedure of designing a set of space-sequential IIR filters with a combined impulse response that approximates the acceleration profile over time. We proceed by segmenting the acceleration profile into sections which have a decaying waveform. We interpret the individual sections as the impulse response from a single filter and find the corresponding IIR filter coefficients with Prony's method [24]. We start our description by considering a single section before introducing our segmentation method. We will illustrate our approach with the acceleration profile from stroking the rubber mat shown in Figure 2(c).

A. Matching the Filter Response to a Segment Profile

Figure 4 shows a section of the acceleration profile over time. The section's start- and endpoint have been selected such that the absolute heights of the local extrema are decreasing, i.e., the overall acceleration wave is decaying. Following the method of Okamura et al. [6], we fit a decaying sinusoid to this waveform in the time-domain for comparison. As discussed earlier, we employ an IIR filter to represent the segment and the decaying sinusoid can be represented as the impulse response of a filter based on Equation 4. Figure 4(a) shows the impulse response of the decaying sinusoid filter. While the decaying sinusoid describes the overall nature of the wave, the fit is quite poor.

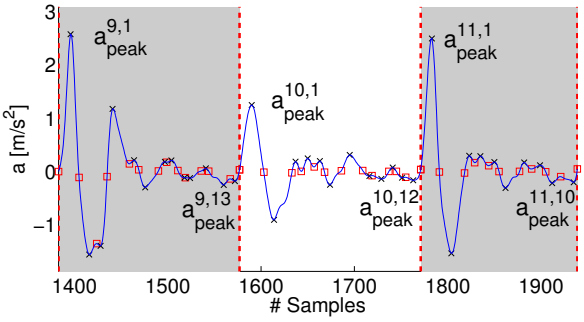

Fig. 5. Segmentation of acceleration profile. The result for segment 10 of the rubber mat (see Figure 2(c)) is shown.

A closer fitting impulse response can be obtained by higher order IIR filters. We employ Prony's method [24] to design such a filter based on the acceleration data. Prony's method is a time domain method for the calculation of the filter coefficients based on the desired impulse response of the filter. The filter corresponds to a Prony's series which is a sum of damped complex exponentials and hence the series is a natural generalization of the decaying sinusoid model. The number of samples of the impulse response required by Prony's method is greater than the sum of the order plus one of the numerator M and denominator N of the filter. However, higher order filters can be used with the help of zero-padding the impulse response. Figure 4(b) shows two results of Prony's method for the same acceleration profile segment as above. The looser fitting curve was estimated by Prony's method with filter order $M = N = 11$, while the tighter fitting curve shown in bold was estimated with a filter order $M = N = 16$. In our method, we start with a filter order equals to the number of extrema of a segment. We increase the order of the filter until the error falls below 1 bit or $0.153\,\mathrm{m/s^2}$ (see Section IV-B for a discussion of sensor quantization noise). A filter order of $N = M = 109$ results in a fit with an error below $1\,\mathrm{mm/s^2}$ which is visually indistinguishable from the original samples in Figure 4(b). As an error measure we use the sum of absolute differences normalized by the number of samples.

B. Segmentation of Acceleration Waveforms

In Section IV-A, we have assumed the existence of a time segment of the acceleration profile consisting of a decaying wave. We have also defined a segment as a section of the profile where the absolute heights of the local extrema are decreasing. It is reasonable to assume that each extremum with a larger absolute magnitude than its predecessor is due to a different surface feature from its predecessor. This assumption is also consistent with the decaying sinusoid model. We therefore segment the acceleration profile (cf. Figure 2) into sections with decaying waveforms.

We find the local extrema of the absolute value of the acceleration profile. The maxima will be the extrema of the signal and since the acceleration profiles are zero-centered, the minima are the start and end locations of a peak (illustrated by the squares in Figure 5). The absolute mimima locations

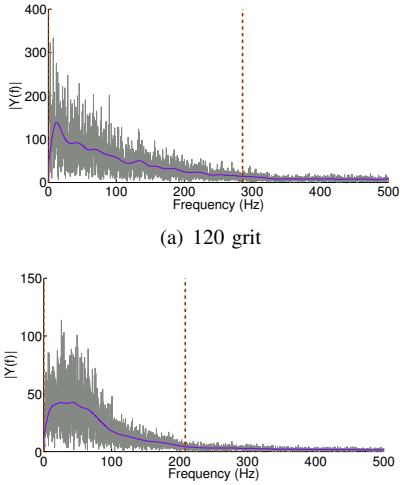

(a) 120 grit

(b) 80 grit

Fig. 6. Acceleration Power Spectrum for Stochastic Texture (Sandpaper).

determine the length of a segment. Each segment starts with the mimima before an absolute peak larger than the previous absolute peak and a segment ends with the minima before an absolute peak larger than the previous absolute peak (see Figure 5). The segmentation criteria are then summarized by $|a_{peak}^{i,1}| > |a_{peak}^{i-1,j_{max(i-1)}}|$ and $|a_{peak}^{i,j_{max(i)}}| < |a_{peak}^{i+1,1}|$ where i is the i^{th} segment in the profile and j is j^{th} absolute maximum within a segment.

Applying the segmentation criteria without taking the noise in the acceleration signal into account leads to a drastic oversegmentation of the acceleration profile. The quantization of the acceleration measurement is one source of noise. The accelerometers used in the WHaT have a range of $\pm 2g$ where $g = 9.81\,\mathrm{m/s^2}$ is the gravitational acceleration which is quantized into 8 bit values. We modify the criteria for the start of a new segment to include a deadband $d = 0.3066\,\mathrm{m/s^2}$ of 2 bits as follows: $|a_{peak}^{i,1}| > |a_{peak}^{i-1,j_{max(i-1)}}| + d$. The deadband is effective in avoiding the creation of short segments in noisy low-signal regions of the scan.

Another source of error consists of inaccuracies in force normalization and the limited bandwidth of the force and acceleration sensors. As a result, the signal during the scanning of a surface feature may result in a too low initial peak in the corresponding acceleration signal. This would result in leading peaks being segmented off a segment corresponding to a feature. We avoid this by using a relative error threshold $|a_{peak}^{i,1}| > |err * a_{peak}^{i-1,j_{max(i-1)}}|$. This works effectively for surface with regular patterns but not for surfaces with stochastic textures. Stochastic textures may have many similar sized peaks (see Figure 2(f)) and a relative error threshold would lead to overly long segments, i.e., it would lead to an under-segmentation. We balance the two competing requirements by reducing the relative error threshold err based on the number of peaks from the beginning of the segments. We choose an exponential decay $err(j) = \alpha * e^{-\beta j}$. We experimentally found values of $\alpha = 1.0$ and $\beta = 0.05$ to work well for all textures captured by us.

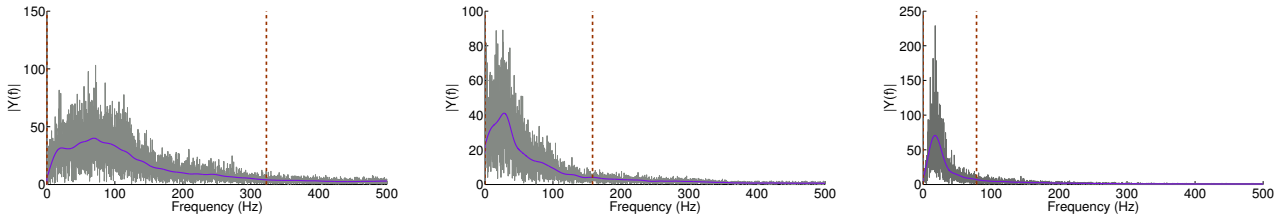

(a) Jewel-case (b) Tire tread (c) Rubber mat

Fig. 7. Acceleration Power Spectrum for Regular Texture.

C. Filtering of Scan Data

The scan data contains high frequency noise and potentially some low frequency drift. The power spectra of the acceleration profiles (see Figures 7 and 6) all exhibit a somewhat similar shape for different textured surfaces but the frequency range and peak frequencies are different. Stiffer material will have more energy in higher frequencies than soft materials due to material damping. We use a bandpass filter to rule out high frequency noise and any remaining low-frequency drift in the acceleration signal. We select the upper limit of the bandpass filter such that at least 75% of the power of the original signal is captured and that no frequency with power larger than 10% of the peak is excluded. Effectively our bandpass filtered signal is now a truthful representation of the measured signal. The upper cutoff frequency is found automatically by low-pass filtering the spectrum and then calculating an upper frequency where

$$\frac{\int_{f_{lower}}^{f_{upper}} |Y(f)|df}{\int_{f_{lower}}^{f_{1/(2T)}} |Y(f)|df} > 0.75 \tag{6}$$

and

$$\forall f > f_{upper} : |Y(f)| < 0.1|Y(f_{major})|. \tag{7}$$

The major frequency f_{major} is the frequency of the peak in the single-sided power spectrum of the acceleration signal after smoothing.

V. Results

We present results for two stochastic surface textures and three textures with a regular pattern, an overview of the raw profiles is shown in Figure 2. We would like to emphasize that these results were obtained by a mobile scanning set-up without any requirement for sampling of the surface. The user follows a free path over the surface and the path is registered with the surface of the object through the visual tracker. Details of the registration process can be found in [13]. The visual tracker results in a position variance between 0.0821 mm and 0.345 mm depending on the measurement direction relative to the camera for a typical scanning set-up [14]. Because of the free scanning no two scans of a surface will exactly follow the same path. This limits our ability to compare repeated scans but we can still observe great similarity between scans of the same surface along similar paths. Below, we will first compare IIR filter models for scans of different materials followed by an analysis of the performance of our model at different rendering velocities. Finally, we give some statistics on the variation of models obtained from repeated scans.

A. IIR Filter Models for Various Surfaces

As discussed in Section IV-B, we first employ a bandpass filter to the raw acceleration profiles. The bandpass filter is a 4^{th}-order Butterworth filter and the upper cutoff frequencies are shown in Table I (lower cutoff is always at 0.122 Hz). We segment the acceleration profile and fit an IIR filter with Prony's method to each segment. The IIR filters obtained with Prony's method have varying degrees depending on the number of extrema per segment and the quality of fit.

The results for surfaces with a regular texture pattern are shown in Figure 8 and the properties of the fit are listed in Table I. The frequency spectrum of the scans varies depending on the stiffness of the scanned surfaces as expected. The rubber mat in Figure 8(c) is the most compliant surface, the tire tread in 8(b) is less compliant while the CD jewel-case in 8(a) is rigid. Correspondingly, our automatic bandpass filter method selects upper cut-off frequencies of 78.6 Hz, 158 Hz and 322 Hz respectively. (The linear coefficients used during force scaling k_c are 0.117, 0.526 and 1.0, respectively, as stated in Section III). The number of segments detected by our method is determined by the approximate number of features encountered during the surface scan. The rim of the CD jewel-case has a very dense texture with ridges located about 1 mm apart while the tire tread and the rubber-mat have bigger features located further apart. However, we will not see these exact distances in our scans since it is practically impossible to scan a textured surface in a straight line by hand. Our novel segmentation routine (Section IV-B) is successful in breaking up the acceleration signal into reasonable segments. For the most part, a single feature corresponds to a single segment and a single filter. Table I shows that the average number of segments per mm is higher for the CD jewel-case than for the tire tread and the rubber mat.

Table I also shows that the residual of our model fit compared to the band-pass filtered profile as well as to the measured complete signal are low. Our fitting approach ensures that the normalized sum of absolute differences between the IIR filter and the bandpass signal of each segment is less than $0.153\,\mathrm{m/s^2}$ which corresponds to 1 bit of the acceleration sensors of the WHaT. While our previous approach [9] of a narrow bandpass filter made it possible to fit the bandpass signal well below the resolution of the sensor with low-order filters, the difference to the measured signal was large because of the many frequencies excluded by bandpass-filtering.

We report our study of stochastic textures based on sandpaper of different grit sizes. The same procedure is used to

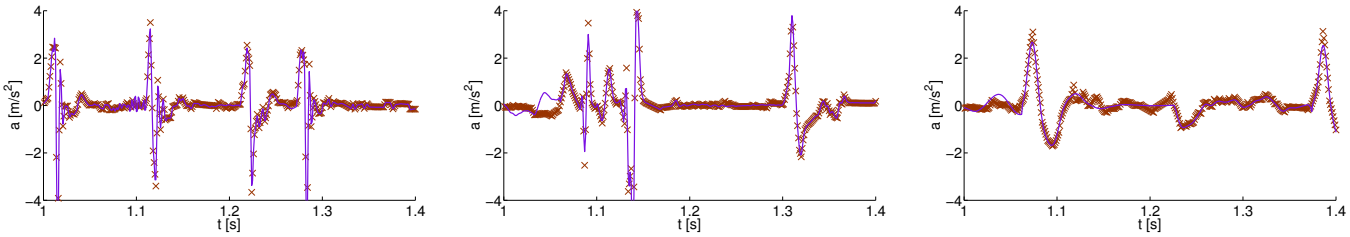

(a) CD jewel case (b) Tire tread (c) Rubber mat

Fig. 8. Patterned haptic textures rendered with the IIR filter model. The IIR filter output is rendered in bold. The measured acceleration data from the WHaT is shown by crosses. The error between bandpass-filtered signal (not shown) and the IIR filter is guaranteed to be less than $0.153 m/s^2$ by the Prony's series fit. See also Table I.

TABLE I
RESULTS FOR THE ESTIMATION OF THE IIR FILTER MODEL.

Object	Texture pattern	f_{max} [Hz]	f_{major} [Hz]	Segment/distance [1/mm]	$\bar{M}+1 = \bar{N}+1$	$\overline{SAD}_{bandpass}$ [mm/s^2]	$\overline{SAD}_{original}$ [mm/s^2]	$\bar{v}_t$ [mm/s]	$\overline{force}$ [N]
Jewel-case	regular	322.8	69.5	1.548	29.5	51.7	84.0	8.2	0.874
Tire tread		133.2	20.6	0.317	35.5	88.9	110.2	20.7	0.511
Rubber mat		78.6	17.8	0.316	29.4	103.9	133.2	21.4	0.443
SP 120 grit	stochastic	285.5	12.6	1.325	12.3	56.3	167.4	23.3	0.636
SP 80 grit		208.0	42.3	1.011	16.7	84.4	110.7	19.9	0.353

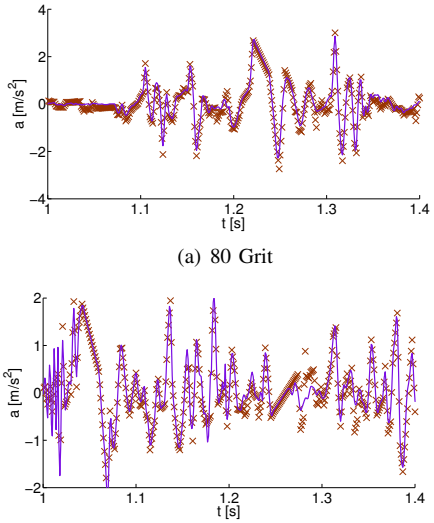

(a) 80 Grit

(b) 120 Grit

Fig. 9. Stochastic haptic textures for sandpaper rendered with the IIR filter model. The IIR filter output is rendered in bold. The measured acceleration data from the WHaT is shown by crosses. The error between bandpass-filtered signal (not shown) and the IIR filter is guaranteed to be less than $0.153\,\mathrm{m/s^2}$ by the Prony's series fit. See also Table I.

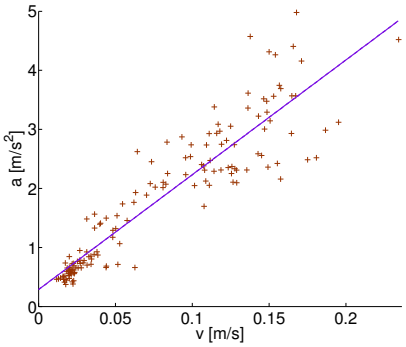

Fig. 10. Dependency of acceleration on tangential velocity during scanning of a rubber mat.

obtain the IIR filters for sandpaper as for the surfaces with regular patterns. Our segmentation routine succeeds with the stochastic textures and breaks up the acceleration profiles despite their inherent stochastic nature. The finer the grit of the sandpaper, the denser the IIR filters should be placed on the surface because the finer grit size results in a larger number of sand particles encountered over a fixed distance. Table I shows that the finer grit sandpaper with 120 grit has a larger number of segments per distance than the coarser 80 grit paper. We have also scanned 220 grit sandpaper but found the grit to be beyond the spatial resolution of our scanning device. Table I also shows that the stochastic textures result in low-order IIR filter models. The acceleration waveform in each segment can be easily approximated by combining only a few complex exponentials during the Prony's series fit.

In summary, our IIR modelling approach with our fitting method succeeds for all three of the regular pattern profiles shown in Figure 8 and the stochastic textures in Figure 9, independent of their characteristics. Nevertheless, some sources of error exist due to the hand-held scanning and also due to the lack of resolution of the sensor. Next, we discuss texture simulation based on our IIR filter model including tangential velocity variations during scanning and rendering as well as the effect of time-aliasing.

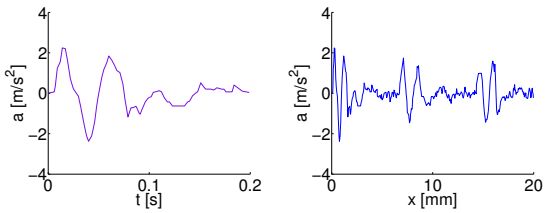

(a) Scanning: Avg. tangential velocity $v_t = 23.7$ mm/s

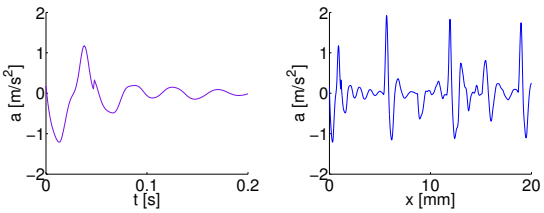

(d) Simulation: Constant velocity $c_t = 23.7$ mm/s

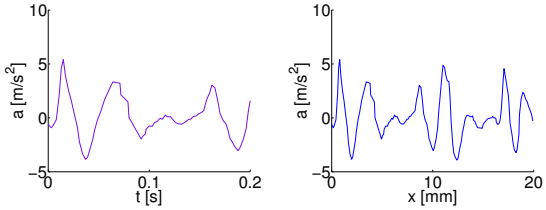

(b) Scanning: Avg. tangential velocity $v_t = 53.7$ mm/s

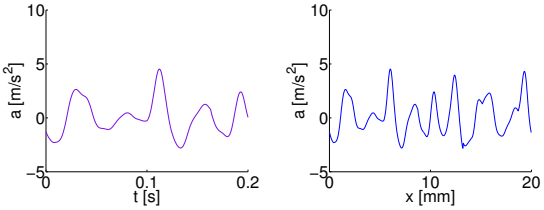

(e) Simulation: Constant velocity $c_t = 53.7$ mm/s

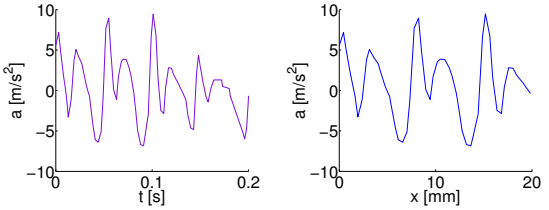

(c) Scanning: Avg. tangential velocity $v_t = 150.3$ mm/s

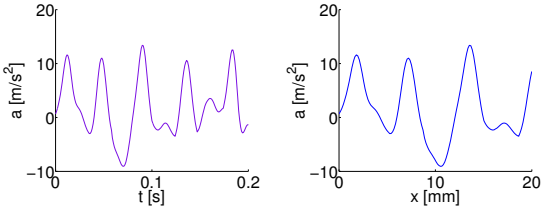

(f) Simulation: Constant velocity $c_t = 150.3$ mm/s

Fig. 11. Influence of tangential velocity on scanned profiles and on haptic textures for the rubber mat. Figures 11(a), 11(b), and 11(c) show scan profiles of the same approximate area on the rubber mat surface with different tangential velocities. Figures 11(d), 11(e), and 11(f) show our haptic texture model for the surface rendered with different velocities. A constant force (0.443 N) is used in the simulation.

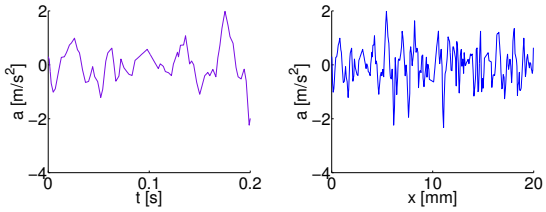

(a) Scanning: Avg. tangential velocity $\bar{v}_t = 29.2$ mm/s

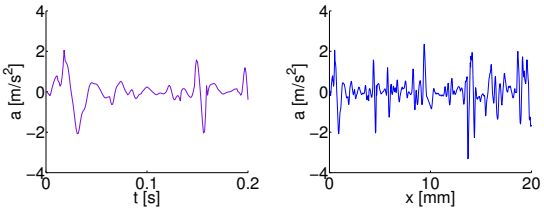

(d) Simulation: Constant velocity $c_t = 29.2$ mm/s

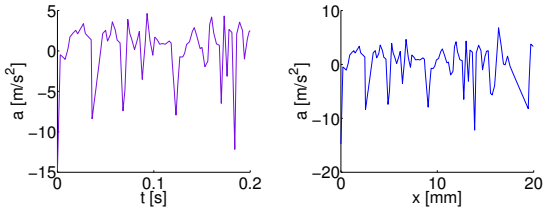

(b) Scanning: Avg. tangential velocity $\bar{v}_t = 78.0$ mm/s

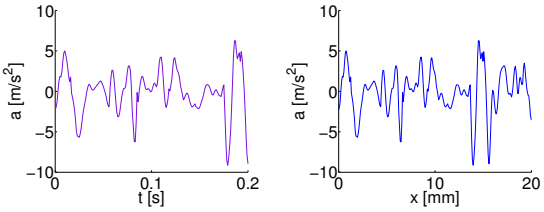

(e) Simulation: Constant velocity $c_t = 78.0$ mm/s

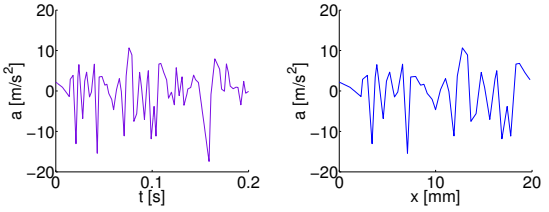

(c) Scanning: Avg. tangential velocity $\bar{v}_t = 172.1$ mm/s

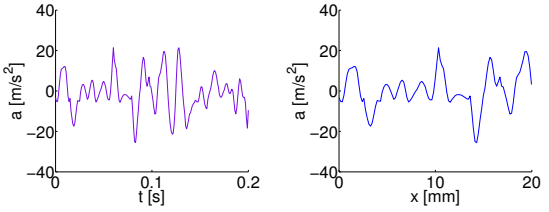

(f) Simulation: Constant velocity $c_t = 172.1$ mm/s

Fig. 12. Influence of tangential velocity on scanned profiles and on haptic textures for 80 grit sandpaper. Figures 12(a), 12(b), and 12(c) show scan profiles of the same approximate area on the sandpaper surface with different tangential velocities. Figures 12(d), 12(e), and 12(f) show our haptic texture model for the surface rendered with different velocities. A constant force (0.353 N) is used in the simulation.

B. Texture Simulation

In this Section, we report simulation results of our IIR filter models. We do not use a standard haptic device for these simulations because of their limited bandwidth. Instead we output the acceleration waveforms to a loudspeaker which can transmit frequencies from approximately 20 Hz to 20 kHz. The user rests the tip of the index finger on the speaker membrane as the membrane vibrates. The vibrations change according to the simulated texture and the simulated contact position but the user cannot influence the rendered position. Besides the large bandwidth of the display, the method has the further advantages that we can directly render a scanned acceleration profile, and that we can render profiles generated with our model with pre-determined velocity. We have not conducted a systematic user study but during informal use, models of different surfaces were clearly distinguishable. Two properties of the surfaces were most noticeable: the stiffness of a material and the spatial frequency of surface features. The stiffness of a material determines the sharpness of individual features while the spatial frequency of surface features and the rendering velocity determine the frequency of features in the acceleration waveform played on the speaker.

We compare in Figures 11 and 12 the acceleration waveforms generated by our method with scanned sections of the same surface for the rubber mat and the 80 grit sandpaper, respectively. We simulate the haptic textures based on our model with a sampling frequency of 1 kHz. We compare the output of our model to three different scanned sections of the same surface. The profiles for the rubber mat in Figure 11 show between three and four large-scale features of the surface in the spatial domain. The large-scale features remain identifiable as the scanning velocity increases, both, in the scans and in the simulation with our model. The time domain profiles show that the decaying waveform between features is not greatly influenced by the scanning or rendering velocity. However, as the velocity increases the features of the surface start to merge, i.e., there is aliasing both, in the scanning of the surface and in the haptic texture simulated by our model. We can conclude that our model behaves as desired since the real world measurements including aliasing are qualitatively matched. The comparison of acceleration waveforms generated by our method and scanned section for the sandpaper in Figure 12 show again a good qualitative correspondence when viewed both, in the time and spatial domain. The aliasing in the spatial domain is also observable.

We vary the amplitude of the acceleration profile generated with our model based on Equation 2. The velocity scaling factor k_v and the offset a_o are estimated by linear regression from repeated scans of the same surface over approximately identical sections and approximately constant velocity during a scan (see Figure 10). We find $k_v = 18.5\,1/\mathrm{s}$, $a_0 = 0.435\,\mathrm{m/s^2}$ and $k_v = 19.4\,1/\mathrm{s}$, $a_0 = 0.287\,\mathrm{m/s^2}$ for the rubber mat and the 80 grit sandpaper, respectively. The force scaling parameter k_c is a result of Lang and Andrews [14].

One limitation of our method is time-aliasing which is encountered during scanning. Time aliasing occurs if one decaying wave has not significantly diminished before the next feature is encountered. Our current segmentation procedure simply starts a new segment with every feature. This effectively truncates the earlier decay and adds the remaining signal to the waveform of the new section. Aliased features can potentially result in missing information if the estimated haptic texture is simulated at a lower velocity than the scanning velocity. We scan therefore the surface as slow as possible if we use the scanned profile for modeling. We were able to produce approximately constant velocities of 21.6 mm/s for the rubber mat and 19.8 mm/s for the 80 grit sandpaper model during scanning by hand. Time aliasing at these low scanning velocities is of little practical concern because these low velocities require human effort and are likely not encountered in virtual reality. Next, we explore the issue of the repeatability of our scanning process.

C. Repeatability of Scans

Above, we have established that our scanning and modelling process produces satisfactory results for the sample textures but we have not studied the repeatability of our approach. In order to quantify the variability between scans, we proceed by scanning each surface five times and comparing the scans. We attempt to follow similar paths for the scans of the individual surfaces but due to the hand-held approach each scan path is slightly different. We report the statistics for filters per scanning distance and filter order in Table II. We also list all parameters of five scans for two surfaces in Table III. The number of segments per scan distance has a reasonable standard deviation for all surfaces. This is an indication that our segmentation approach generates segments which correspond to features of the surface. The filter order of the IIR filter has some variation. It is well known that estimating a Prony's series from noisy data can lead to instabilities in the parameters of the series. In particular, for some sections of the profile a high filter order is needed to achieve the prescribed error threshold. A more elaborate stopping criterion for determining the order of the Prony's series, e.g., based on a combination of approximation error and filter order relative to segment size may be advantageous. However, for our application the parameter of the Prony's series including the filter order are less important than the approximation error. The approximation error measured by the normalized sum of absolute differences with respect to the bandpass filtered signal $\overline{SAD}_{bandpass}$ and with respect to the original signal

TABLE II
IIR FILTER ORDER AND SEGMENT LENGTH FOR SCANS OF DIFFERENT SURFACES.

Object	Segments/length [1/mm]		$\bar{M}+1=\bar{N}+1$	
	Mean	σ	Mean	σ
Jewel-case	1.637	0.270	23.31	5.39
Tire tread	0.359	0.098	39.41	2.81
Rubber mat	0.345	0.031	31.06	6.14
SP 120 grit	1.181	0.132	14.43	2.72
SP 80 grit	1.030	0.066	17.71	3.63

TABLE III
IIR FILTER MODEL FROM MULTIPLE SCANS.

Object	Scan	f_{max} [Hz]	f_{major} [Hz]	Segment/distance [1/mm]	$\bar{M}+1 = \bar{N}+1$	$\overline{SAD}_{bandpass}$ [mm/s^2]	$\overline{SAD}_{original}$ [mm/s^2]	$\bar{v}_t$ [mm/s]	$\overline{force}$ [N]
Rubber mat	1	91.4	18.7	0.373	33.2	91.7	138.0	19.1	0.439
	2	79.5	18.6	0.365	24.9	105.0	134.7	21.4	0.624
	3	78.6	17.8	0.316	29.4	103.9	133.2	21.4	0.443
	4	79.0	17.2	0.307	27.2	105.8	139.3	25.3	0.477
	5	86.9	17.5	0.366	40.6	92.9	147.9	17.5	0.525
SP 80 grit	1	190.6	25.9	0.992	13.5	89.9	168.1	22.6	0.187
	2	208.0	42.3	1.011	16.7	84.4	110.7	19.9	0.353
	3	286.7	49.4	1.146	20.1	76.9	112.9	15.1	0.385
	4	197.3	32.9	0.985	22.6	75.2	95.8	15.1	0.344
	5	217.5	24.4	1.014	15.7	82.3	125.5	21.1	0.143

$\overline{SAD}_{original}$ is consistently low as shown in Tables I and III. We also did not perceive the high filter order sections during rendering and hence did not investigate a more advanced stopping criterion for the Prony's series fit further.

Table III shows that the different scans have been acquired with slightly different velocities and forces. (The velocity is estimated based on visual tracking). The comparison shows that the raw scans have a similar major frequency for the rubber mat but not for the 80 grit sandpaper. This is not surprising considering the pattern of the rubber mat texture and the stochastic nature of the sandpaper (see also the power spectrum in Figure 6(b)). Our method to estimate the upper cut-off frequency of the bandpass filter results in some variability but the difference in the bandpass filtered signals are not noticeable.

VI. CONCLUSION

In this paper we develop a novel method to obtain vibrotactile textures from real-world samples. Our novel texture model consists of spatially distributed and computationally efficient IIR filters which operate in the time-domain. During haptic rendering of the proles, the user can traverse the textured surface at any speed, and the spatial frequencies of the features remain constant, but damping is xed in time, i.e., the spatial extent of the damping waveform varies with velocity. Our procedure extends and unifies the decaying sinusoid approach which has been proposed by others previously. Our estimation method is able to estimate suitable IIR filters for stochastic, patterned and mixed surfaces. The method is based on fully-automatic segmentation of the acceleration signal and the use of Prony's method for filter design. We showed that the method is stable for repeated scans of a surface despite scanning variations introduced by our hand-held scanning approach. In future work, we would like to employ our models to characterize different surfaces for recognition and to synthesize new models for virtual textures.

ACKNOWLEDGEMENT

The authors gratefully acknowledge the financial support from the Natural Sciences and Engineering Research Council of Canada (NSERC).

REFERENCES

[1] W. McMahan and K. J. Kuchenbecker, "Haptic display of realistic tool contact via dynamically compensated control of a dedicated actuator," in *Proc. IEEE Intelligent Robots and Systems Conference (IROS)*, St. Louis, USA, Oct 2009, pp. 3171–3177.

[2] D. Pai, J. Lang, J. Lloyd, and R. Woodham, "Acme, a telerobotic active measurement facility," in *6th Int. Symp. on Exp. Robotics*, Sydney, Australia, Mar 1999, pp. 391–400.

[3] R. Klatzky and S. Lederman, "Tactile roughness perception with a rigid link interposed between skin and surface," *Perception & Psychophysics*, vol. 61, no. 4, pp. 591–607, 1999.

[4] V. Hayward and K. Maclean, "Do it yourself haptics: part I," *IEEE Robotics & Automation Magazine*, vol. 14, no. 4, pp. 88–104, 2007.

[5] P. Wellman and R. Howe, "Towards realistic vibrotactile display in virtual environments," *ASME Dynamic Systems and Control Division*, vol. 57, no. 2, pp. 713–718, 1995.

[6] A. Okamura, J. Dennerlein, and R. Howe, "Vibration feedback models for virtual environments," in *Proc. IEEE Intl. Conf. Robotics and Automation*, 1998, pp. 674–679.

[7] K. Kuchenbecker, J. Fiene, and G. Niemeyer, "Improving contact realism through event-based haptic feedback," *IEEE Transactions on Visualization and Computer Graphics*, vol. 12, no. 2, pp. 219–230, 2006.

[8] N. Abolhassani, R. Patel, and M. Moallem, "Needle insertion into soft tissue: A survey," *Medical Engineering & Physics*, vol. 29, no. 4, pp. 413–431, 2007.

[9] V. Guruswamy, J. Lang, and W. Lee, "Modelling of haptic vibration textures with infinite-impulse-response filters," in *IEEE Int. Workshop on Haptic, Audio-Visual Env. and Games (HAVE)*, Lecco, Italy, Nov 2009.

[10] K. Kuchenbecker, J. Romano, and W. McMahan, "Haptography: Capturing and recreating the rich feel of real surfaces," in *Proc. 14th Int. Symp. on Robotics Research*, Lucerne, Switzerland, Aug 2009.

[11] J. Romano, T. Yoshioka, and K. Kuchenbecker, "Automatic filter design for synthesis of haptic textures from recorded acceleration data," in *IEEE Int. Conf. on Robotics and Automation*, Anchorage, USA, May 2010.

[12] D. Pai and P. Rizun, "The WHaT: A wireless haptic texture sensor," in *Proc. 11th Symp. on Haptic Interfaces for Virtual Environment and Teleoperator Systems*, Los Angeles, USA, 2003.

[13] S. Andrews and J. Lang, "Interactive scanning of haptic textures and surface compliance," in *Proc. 6th Int. Conf. on 3-D Digital Imaging and Modeling*, Aug. 2007, pp. 99–106.

[14] J. Lang and S. Andrews, "Measurement-based modeling of contact forces and textures for haptic rendering," *IEEE Trans. on Visualization and Computer Graphics*, to appear, DOI 10.1109/TVCG.2010.52.

[15] S. Baglio, G. Muscato, and N. Savalli, "Tactile measuring systems for the recognition of unknown surfaces," *IEEE Trans. on Instrumentation and Measurement*, vol. 51, no. 3, pp. 522–531, 2002.

[16] E. Petriu, W. McMath, S. Yeung, and N. Trif, "Active tactile perception of object surface geometric profiles," *IEEE Trans. on Instrumentation and Measurement*, vol. 41, no. 1, pp. 87–92, 1992.

[17] M. Minsky, O.-Y. Ming, O. Steele, J. F.P. Brooks, and M. Behensky, "Feeling and seeing: issues in force display," in *Proc. Symp. on Interactive 3D Graphics*. ACM Press, 1990, pp. 235–241.

[18] J. Siira and D. Pai, "Haptic rendering: A stochastic approach," in *Proc. 1996 IEEE Intl. Conference Robotics and Automation*, 1996, pp. 557–562.
[19] C. Basdogan, C. Ho, and M. Srnivasan, "A ray-based haptic rendering technique for displaying shape and texture of 3d objects in virtual environment," in *Proc. Of the ASME Dynamic Systems and Control Division*, 1997, pp. 77–84.
[20] S. Wall and W. Harwin, "Modelling of surface identifying characteristics using fourier series," in *Proc. Symp. on Haptic Interfaces for Virtual Environments and Teleoperators*, 1999, pp. 65–71.
[21] M. Costa and M. Cutkosky, "Roughness perception of haptically displayed fractal surfaces," *Proc. of the ASME Dynamic Systems and Control Division*, vol. 69, no. 2, pp. 1073–1079, 2000.
[22] W. McMahan, J. Romano, A. A. Rahuman, and K. Kuchenbecker, "High frequency acceleration feedback significantly increases the realism of haptically rendered textured surfaces," in *IEEE Haptics Symposium*, Waltham, MA., USA, Mar 2010, pp. 141–148.
[23] S. Andrews and J. Lang, "Haptic texturing based on real-world samples," in *Proc. IEEE Int. Workshop on Haptic Audio Visual Environments and their Applications: HAVE*, October 2007.
[24] T. Parks and C. Burrus, *Digital Filter Design*. John Wiley & Sons, 1987.

Vijaya Lakshmi Guruswamy completed her Bachelors of Engineering Degree at a college affiliated to Anna University, Chennai, India in 2006. She attained her Masters degree in Computer Science from the University of Ottawa, Ontario, Canada in 2009. Her thesis research work was focused on vibration based texture models for haptics. Her research interests include computer graphics and animation, mathematical models for signal processing and virtual reality applications. Currently she is employed as an IT Consultant with Compuzonic in Ottawa, Ontario, Canada.

Jochen Lang received the M.Sc. degree in computer science from York University, Toronto, Canada and the Ph.D. degree in computer science from the University of British Columbia, Canada in 2001. From 2002 to 2004, he was a Postdoctoral Researcher at the Max-Planck-Institut für Informatik, Saarbrücken, Germany. Currently, he is an Associate Professor with the School of Information Technology at the University of Ottawa, Canada where he is a member of the Distributed and Collaborative Virtual Environments Research Laboratory (DISCOVER) and the VIVA laboratory. His research focuses on measurement-based modelling in the areas of computer graphics and computer haptics. He is working on image-based models, 3D model acquisition, textures and deformable models. He is a member of the IEEE.

Dr. Won-Sook Lee , associate professor in the School of Information Technology and Engineering, Faculty of Engineering at University of Ottawa, Canada, received her PhD from the University of Geneva, Switzerland. She has both industrial and academic experiences in Korea, Singapore, Switzerland, USA and Canada. She has wide research interests in the fields of computer graphics and related application areas such as computer animation, computer game, virtual reality, and medical imaging as well as haptic graphics. She has over 60 peer reviewed publications.